Glassy Dielectric Response in Tb_2NiMnO_6 Double Perovskite with Similarities to a Griffiths Phase

Hariharan N.*,[1, a)] Harikrishnan S. Nair*,[2, 1, b)] H. L. Bhat,[1, 3] and Suja Elizabeth[1]
[1)] *Department of Physics, Indian Institute of Science, Bangalore 560012, India*
[2)] *Jülich Center for Neutron Sciences and Peter Grünberg Institute, JARA-FIT, Forschungszentrum Jülich GmbH, 52425 Jülich, Germany*
[3)] *Center for Soft Mater Research, Jalahalli, Bangalore 560013, India*

(Dated: 23 December 2013)

Frequency-dependent and temperature-dependent dielectric measurements are performed on double perovskite Tb_2NiMnO_6. The real (ϵ_1) and imaginary (ϵ_2) parts of dielectric permittivity show three plateaus suggesting dielectric relaxation originating from bulk, grain boundaries and the sample-electrode interfaces respectively. The temperature and frequency variation of ϵ_1 and ϵ_2 are successfully simulated by a RC circuit model. The complex plane of impedance, Z'-Z", is simulated using a series network with a resistor R and a constant phase element. Through the analysis of frequency-dependent dielectric constant using modified-Debye model, different relaxation regimes are identified. Temperature dependence of dc conductivity also presents a clear change in slope at, T^*. Interestingly, T^* compares with the temperature at which an anomaly occurs in the phonon modes and the Griffiths temperature for this compound. The components R and C corresponding to the bulk and the parameter α from modified-Debye fit tend support to this hypothesis. Though these results cannot be interpreted as magnetoelectric coupling, the relationship between lattice and magnetism is marked.

I. INTRODUCTION

Double perovskite compounds $R_2BB'O_6$ (R = rare earth; B, B' = transition metal) display a variety of interesting properties such as ferromagnetism[1], magnetocapacitance/ magnetoresistance[2] and field-induced changes of dielectric constant[3] all which make them potential candidates for spintronics applications. Theoretical predictions[4] and experimental observation[5] of multiferroicity have been reported for double perovskites. However, most investigations of this class of compounds were focused on La-based compositions, for example, La_2NiMnO_6 which has a high ferromagnetic transition temperature of 280 K[6,7]. Ceramics of La_2NiMnO_6 are reported to show relaxor-like dielectric response which is attributed to Ni^{2+} – Mn^{4+} charge ordering[7]. Epitaxial thin films of La_2NiMnO_6 are known for dielectric relaxation and magnetodielectric effect[6]. In the present paper, we report the results of impedance spectroscopy of Tb_2NiMnO_6. The motivation for the this work stems from our previous studiy that showed a clear correlation between lattice anomaly observed in FWHM of phonon mode and Griffiths temperature observed through magnetization[8]. Here we address the dielectric response of this system, its interpretation and appraisal based on the previous knowledge. Experimentally observed dielectric data is faithfully reproduced using resistor network models which help to extract intrinsic contributions. A characteristic temperature is identified in the ensuing analyses which is compared with the magnetic and Raman data already reported on this material.

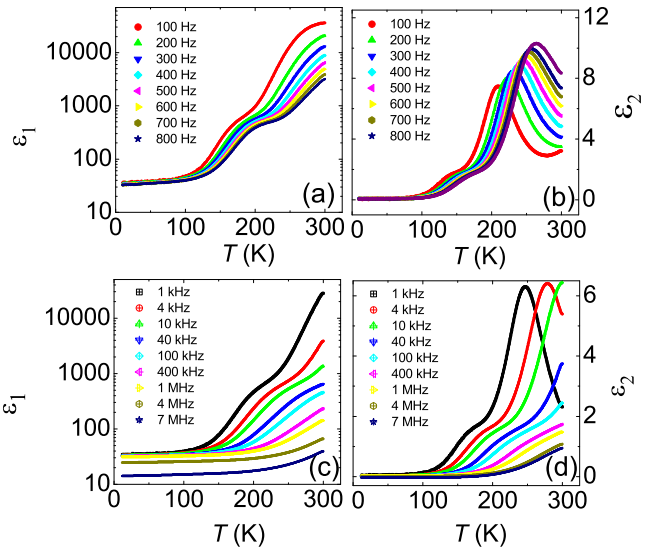

FIG. 1. (colour online) The real part of dielectric permittivity, ϵ_1, and the dissipation factor or loss, ϵ_2, as a function of temperature, measured with different applied frequencies in the range 100 Hz – 800 Hz (a, b) and 1 kHz – 7 MHz (c, d). In the low frequency region, three different plateaus are observed which can arise from intrinsic, grain boundary and sample-electrode interfaces respectively.

It is found that the magnetic Griffiths temperature is reflected in the dielectric data also through this characteristic temperature.

[a)] Electronic mail: hariharan.nhalil@gmail.com
[b)] h.nair@fz-juelich.de, krishnair1@gmail.com* authors contributed equally to the work

II. EXPERIMENTAL DETAILS

Details of synthesis, structure, magnetism and Raman studies of Tb_2NiMnO_6 were reported earlier[8]. In order to perform dielectric measurements, pellets of approximate thickness 0.8 mm and area 6.8 mm^2 were prepared using poly-vinyl alcohol as a binder. Density of the pellet is measured to be greater than 95 % of the theoretical density. Temperature dependent dielectric constant was measured using a Janis cryostat in the frequency range 1 kHz to 10 MHz using a 4294A precision impedance analyser with an applied ac voltage of 800 mV. Dielectric experiments on these samples were repeated using several electrodes. Initially, silver paste was applied on both sides of the pellet and was baked at 250°C for 3-4 hours before measurement. Afterwards, the measurements were repeated using silver and gold plated electrodes. The data obtained with all the three types of electrodes were consistent.

III. RESULTS AND DISCUSSION

The temperature dependence of real and imaginary parts of dielectric permittivity, $\epsilon_1(f,T)$ and $\epsilon_2(f,T)$ of Tb_2NiMnO_6 in the frequency region, 100 Hz-800 Hz is shown in Fig 1 (a, b) and for the range, 1 kHz-7 MHz in Fig 1 (c, d). Clear frequency dispersion is observed in both plots $\epsilon_1(f,T)$ and $\epsilon_2(f,T)$ and a closer examination reveals different plateaus. Schmidt *et al*[9] have shown that each relaxation is represented by a dielectric plateau, three of which are indeed seen at low frequencies (Fig1(a)). At high frequencies (Fig1(c)) the third plateau is not observed. The low-temperature plateau originates from the intrinsic bulk contribution and the high temperature plateaus could be due to the grain boundaries and sample-electrode interface.[10,11] Each relaxation can be ideally represented by one RC element[12] where R and C connected in parallel, and three RC elements in series (upper panel of Fig 2) was used to model the real and imaginary part of the permittivity versus T and frequency dependence.

The complex impedance is given by[13]

$$Z^* = Z' + iZ" \tag{1}$$

where Z' and $Z"$ are real and imaginary part of the Z^* respectively.

For a series of three RC elements as shown in Fig 2, the real and imaginary part of the permitivity are calculated[9] as ,

$$Z^* = \frac{R_1}{1+i\omega R_1C_1} + \frac{R_2}{1+i\omega R_2C_2} + \frac{R_3}{1+i\omega R_3C_3} \tag{2}$$

$$\epsilon_1 = \frac{-Z"}{\omega\epsilon_0 g\,(Z'^2 + Z"^2)} \tag{3}$$

$$\epsilon_2 = \frac{Z'}{\omega\epsilon_0 g\,(Z'^2 + Z"^2)} \tag{4}$$

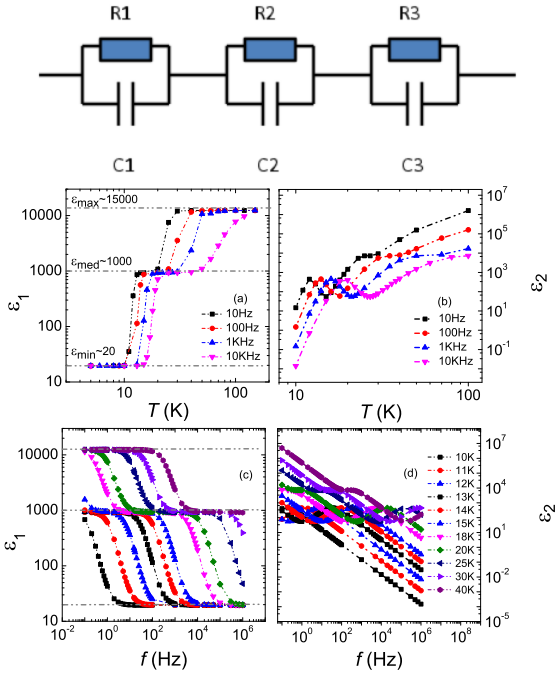

FIG. 2. (colour online) *Top:* The schematic of the RC circuit used for simulating ϵ_1 and ϵ_2 versus temperature plots for different frequencies. *Bottom:* Simulated curves of (a) ϵ_1 and (b) ϵ_2 versus temperature for different frequencies. As clear from (a), three plateau-regions corresponding to ϵ_{min}, ϵ_{med} and ϵ_{max} are present in the experimental data also (Fig 1 (a, b)). Simulated curves of ϵ_1 and ϵ_2 as a function of frequencies for different temperatures are shown in (c) and (d).

where ω is the angular frequency of the applied ac voltage and ϵ_0 is the permittivity of free space and g is a geometrical factor ($\propto$ area/ thickness). In equation (2), R_1C_1 represent the intrinsic contribution while R_2C_2 and R_3C_3 are the external contributions from the grain boundaries and the sample-electrode interface respectively. Initially all capacitances are treated as temperature independent and the resistors obey Arrhenius type activated behavior[9] $R_n = a_n \exp(20\ \text{meV}/k_B\text{T})$. Assuming $R_3 \gg R_2 \gg R_1$, the pre-exponential constants a_1, a_2 and a_3 are taken as 1, 1000, and 10000 respectively. The capacitance values used for the simulation are calculated from the experimentally observed plateaus of ϵ_1 vs T plots, which yielded $C_1 = 1.76$ pF ($\epsilon_{low} = 20$), $C_2 = 88.4$ pF ($\epsilon_{med} = 100$), and $C_3 = 1.326$ nF ($\epsilon_{max} = 15000$). The simulated plots for real and imaginary part of the permittivity are shown in Fig 2 (a, b). The real part, ϵ_1, has three plateaus in accordance with the three types of relaxations. The the bulk, grain boundaries and third from the sample electrode interface[9,11]. If temperature is lowered the intrinsic contribution dominates and at sufficiently low T, the extrinsic contributions ceases (fig 2 (c)). The imaginary part ϵ_2 has two peaks which is similar to the experimental

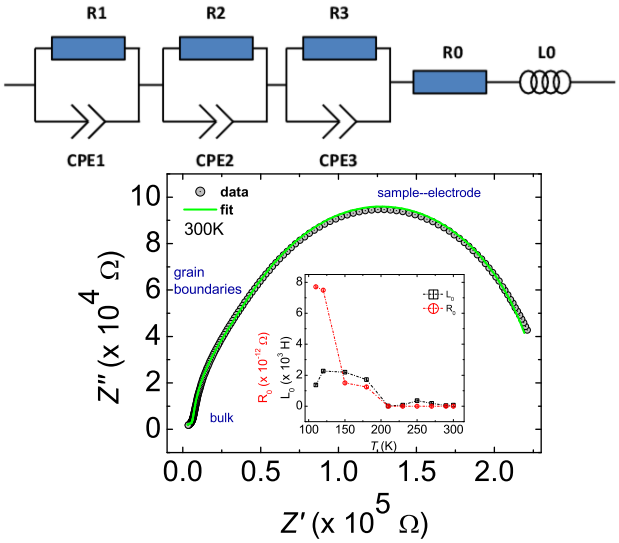

FIG. 3. (colour online) *Top:* The *R-CPE* circuit used to model the complex plane of impedance, Z' vs Z". *Bottom:* The experimental Z' vs Z" plot at 300 K shown as circles. A fit to the observed data according to the circuit model shown above is given as solid line. The three different contributions to the total relaxation are marked. The inset shows the temperature dependence of R_0 and L_0 (in the circuit) extracted from the fit. A clear divergence in slope is seen in both R_0 and L_0 around 200 K.

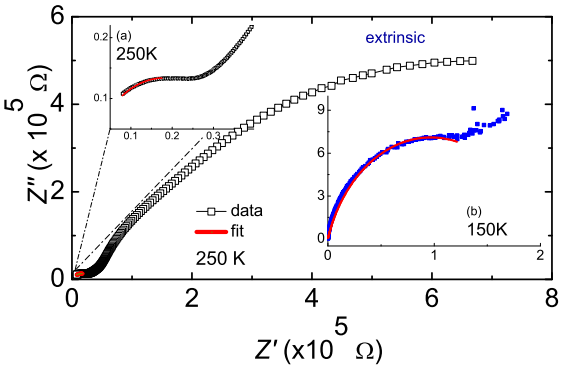

FIG. 4. (color online) The complex plane of Z' vs Z" at 250 K. The inset (a) shows an enlarged view of the region where bulk contribution (red line) dominates. The data and fit at 150 K is shown in the inset (b).

data (Fig1(b) and (d)). These features are also reflected in the simulated frequency dependent dielectric constant, Fig 2(c) and (d).

Impedance spectroscopy is a very powerful tool to study the multiple relaxations observed in dielectric materials, where the real (Z') versus imaginary (Z") part of the complex impedance for different frequencies are plotted together. Subsequent analysis using RC element model can deconvolute different types of dielectric relaxations present in the material.[13] In the ideal case of single relaxation, the response is a semi-circle.[14] In real systems, deviation from ideal behaviour occur and in order to account for this non-Debye type behavior, the ideal capacitor is replaced with a Constant Phase Element (CPE). The complex impedance of a CPE is defined as[9,15]

$$Z^*_{CPE} = \frac{1}{C_{CPE}(i\omega)^n} \qquad (5)$$

where C_{CPE} is the CPE-specific capacitance. ω is the angular frequency and n is a critical exponent with typical values between 0.6 and 1 (for ideal capacitor $n = 1$). Such CPE capacitance can be converted into real capacitance using standard procedure.[16] . Such a circuit model constructed for the present work is illustrated in the top panel of Fig 3. The impedance of the sample is measured at different temperatures and Z" versus Z' are plotted. The room temperature impedance spectra in the complex plane is shown in Fig 3 as black open circles. The data are fitted using three *R-CPE* units in series corresponding to the bulk, the grain boundary and the sample-electrode contributions. The inductance L_0 of the external leads (also related to the magnetic phase) and the resistance, R_0, of the leads and electrodes are also taken into account in the circuit model. The curve fit to the experimental data at 300 K using this equivalent circuit is shown in Fig 3 as solid line. The fit parameters are $R_1 = 6467$ ±23% ohm, $R_2 = 23625$ ±9% ohm, $R_3 = 200860$ ±1.9% ohm, $C_1 = 5.33$ nF ±2.9%, $C_2 = 1.62$ nF ±2.6% , $C_3 = 2.39$ pF ±2.1%, $n_1 = 0.79$ ±1.1%, $n_2 = 0.98$ ±2.4% and $n_3 = 0.95$ ±1.8%. The high frequency response originates normally from the bulk, the intermediate frequency from the grain boundaries and the low frequency impedance contribution from the sample-electrode interface.[12] Impedance data of magnetic materials are usually modeled by including an inductive element in the equivalent circuit wherein the permiability and magnetic response can be roughly understood from the inductance.[17,18] A combination of R and L (parallel or series) are generally used for modeling the magnetic phase.[17,19] Using the circuit shown in fig 3 we tried to extract the temperature dependence of inductance L_0 along with R_0 and is shown in the inset of bottom panel of fig 3. A clear anomaly is observed around 200 K which is close to the Griffith's temperature observed in this material[8]. Irvin *et al.,* for example, have observed that the inductance value peaks at the magnetic anomaly transitions in $(NiZn)Fe_2O_4$.[17]

The intrinsic bulk contribution is analyzed using a single *R-CPE* unit by considering the intermediate and low frequency region as extrinsic. The data is fitted faithfully upto 110 K. Fig 4 shows the fit at 250 K (inset (a))and 150 K (inset (b)). At low temperature the bulk contribution dominates and the extrinsic contribution re-

duces. By a progressive procedure of fitting, the intrinsic response to the dielectric relaxation was extracted. The resistance (R) and the capacitance (C) estimated from the fit are plotted against temperature, Fig 5. A slope change is visible in the temperature region around 200 K which coincides with the experimentally observed Griffith's temperature in this compound.[8] The spin-lattice coupling also shows a marked change at this point. Although one cannot claim this to be magneto-electric coupling, it certainly indicate a connection between the various degrees of freedom. For ideal Debye relaxation of non-interacting dipoles, the plot of $\epsilon_1(T)$ versus $\epsilon_2(T)$ follows Cole-Cole behaviour displaying a perfect semicircular arc[20]. Like in many complex oxides and those with defects, deviations from ideal Cole-Cole plot are observed here; these may be accounted by using the modified-Debye equation,

$$\epsilon^* = \epsilon_1 + i\epsilon_2 = \epsilon_\infty + \frac{(\epsilon_0 - \epsilon_\infty)}{[1 + (i\omega\tau)^{(1-\alpha)}]} \qquad (6)$$

where ϵ_0 and ϵ_∞ are static and high frequency dielectric constants, respectively, ω is the angular frequency, τ is the mean relaxation time and α is a parameter which represents the distribution of relaxation times (for ideal Debye relaxation, α is zero). Equation (6) can be separated into the real and imaginary part of dielectric permittivity as,

$$\epsilon_1 = \epsilon_\infty + (\Delta\epsilon/2)[1 - \frac{\sinh(\beta z)}{\cosh(\beta z) + \cos(\beta\pi/2)}] \qquad (7)$$

$$\text{and,} \quad \epsilon_2 = \frac{(\Delta\epsilon/2)\sin(\beta\pi/2)}{\cosh(\beta z) + \cos(\beta\pi/2)} \qquad (8)$$

where $\Delta\epsilon$ = (ϵ_0 - ϵ_∞), z = ln($\omega\tau$) and β = (1 - α). The frequency dependence of $\epsilon_1(T)$ for Tb_2NiMnO_6 at few select temperatures is depicted in Fig 6 along with the curve fits using modified-Debye equation (Eqn 7). Since bulk contribution will reflect in the high frequency region, fitting was performed in the high frequency region. However, the modified-Debye model was inadequate to describe the behaviour of ϵ_1 below 120 K (fig not shown) and attempts to fit Eqn (7) were not successful. The value extracted for α from the fit falls between 0.27 – 0.18 which is higher than the value reported for La_2NiMnO_6[7]. Inset of fig 6 (b)shows the temperature variation of α values extracted from the fit. An anomaly in the behavior is observed in the vicinity of $\sim$ 200 K. We denote the temperature at which the deviation occurs as T^*, which is close to the temperature where an anomaly in the FWHM of Raman modes was observed in Tb_2NiMnO_6 (180 K)[8]. This coincidence gives credence to the correlation between dielectric, Raman and magnetic anomalies in this material.

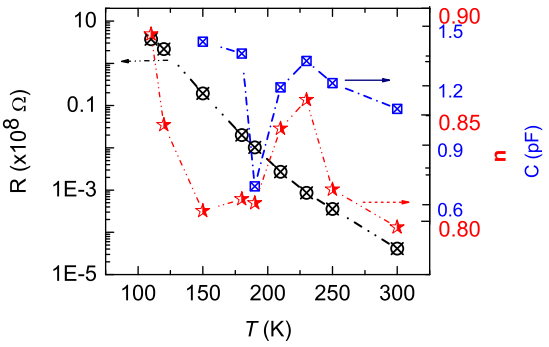

FIG. 5. (colour online) The estimated values of R, C and n by separating the intrinsic dielectric relaxation after analysis using the resistor-capacitor models. A broad anomaly is present centered around 200 K (the error bars were comparable to the size of the data points).

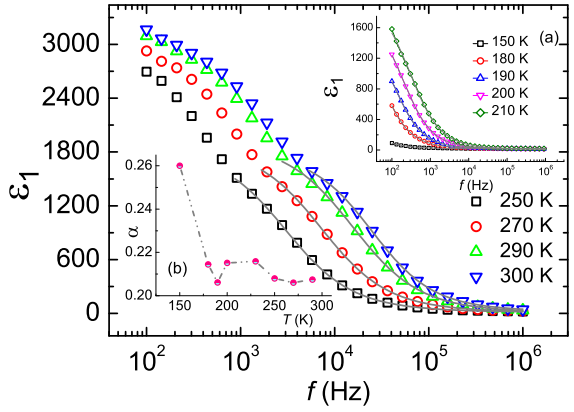

FIG. 6. (colour online) Frequency dependence of real part of dielectric constant, $\epsilon_1(T)$, at different temperatures above $T^* \approx$ 200 K. The inset (a) shows $\epsilon_1(T)$ below 250 K. The solid lines are fits using modified-Debye equation, Eqn 7. The behaviour of dielectric function is clearly different for temperatures above and below T^*. The inset (b) shows the variation of α with temperature across T^*.

The frequency dependence of ac conductivity σ of Tb_2NiMnO_6 is shown in Fig 7 (a) and (b). This corresponds to two types of conduction behaviour at $T < T^*$ and $T > T^*$. Below 200 K, conductivity decreases with increase in temperature reflecting an insulating behaviour. A change of slope in ac conductivity occurs at the temperature where dielectric relaxation deviates from Debye-like behaviour. According to universal dielectric response (UDR),[15] the relation between conductivity $\sigma'(f)$ and dielectric constant ϵ_1 is given by,

$$\sigma'(f) = \sigma_{dc} + \sigma_0 f^s \qquad (9)$$

and,

$$\epsilon_1 = \tan(s\pi/2)\sigma_0 f^{s-1}/\epsilon_0 \qquad (10)$$

where, f is the experimental frequency, σ_0 and s are temperature dependent constants. A step wise increase in the background of loss factor reveals the contribution from dc conductivity (fig 1 (b) and (d)). Equation (10) can be written as,

$$f\epsilon_1 = A(T)f^s \qquad (11)$$

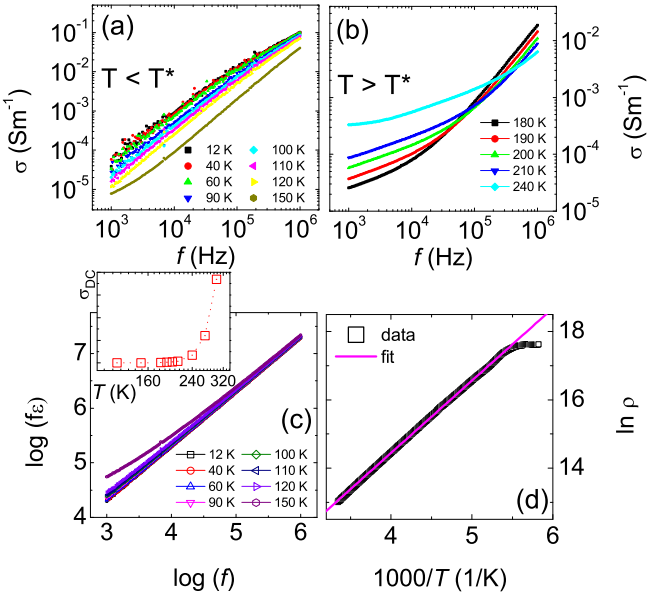

FIG. 7. (colour online) (a) Shows the frequency dependence of ac conductivity below $T^* \sim 200$ K. (b) Frequency dependence of ac conductivity at temperatures above T^*. (c) Plot of log $(f\epsilon_1')$ vs log (f) for selected fixed temperatures. The inset presents temperature evolution of dc conductivity which shows a significant change in slope close to 200 K. (d) Electrical resistance of Tb_2NiMnO_6 which conforms to Arrhenius type behaviour.

where, $A(T) = \tan(\frac{s\pi}{2})$ $(\frac{\sigma_0}{\epsilon_0})$, a plot of $\log(f\epsilon_1)$ vs $\log(f)$ results in a straight line with slope equal to s. This is presented in Fig 7 (c) where a clear straight line is observed at low temperatures. However, it deviates from linearity as temperature increases above $T^* \approx 200$ K, when charge carriers contribute to polarization. In order to find the dc contribution, the low frequency ac conductivity was extrapolated to zero frequency. The dc conductivity of Tb_2NiMnO_6 relates to semiconducting like behaviour above 200 K but deviates from thermally activated behaviour. The variation of dc conductivity, σ_{DC}, with temperature is shown in the inset of Fig 7 (c) where the change in slope is clearly visible close to 200 K. Again, the characteristic temperature $T^* \sim 200$ K compares well with the the reported anomaly in the FWHM of Raman modes[8]. Figure 7 (d) shows the electrical resistivity of Tb_2NiMnO_6 plotted in log scale against 1000/T. The resistivity data fits reasonably well to the Arrhenius law up to ~ 200 K. This supports the dc conductivity data derived from the ac conductivity and yields activation energy, $E_a = 0.192(1)$ eV.

In our previous work concerning magnetic properties of Tb_2NiMnO_6, an inhomogeneous magnetic state resembling Griffiths phase was observed along with clear indications of spin-lattice coupling through Raman studies.[8] We were able to extract a characteristic temperature $T^* \approx 200$ K where magnetic and Raman anomalies coincided. The present dielectric response study validated by the dielectric relaxation and the ensuing impedence and conductivity behavior reflect the same characteristic temperature T^* in this compound. Diffuse dielectric behaviour has been observed in nanoparticle samples of the double perovskite La_2NiMnO_6 where disorder leads to local polar nanoregions[21] and also in La_2CoMnO_6 ceramics[22] where the charge order of Co^{2+} and Mn^{4+} was the origin of relaxation. It could be assumed, in th epresent case, that clusters that posses local polarization (polar nanoregions) are formed around Ni^{2+} or Mn^{4+} due to the cationic antisite disorder and bring about dielectric relaxation through their mutual interaction. This is also supported by the fact that the frequency dependence of the peak temperatute in dielectric data is not explained by thermally activated behaviour. Similar to the magnetic Griffiths phase where the nonanalyticity of magnetization extends above the transition temperature (in the present case, $T_c \approx 110$ K), the dielectric relaxation also identifies the characteristic temperature above T_c. In this context, it would be intersting to perform experimental investigations using local probes like electron paramagnetic resonance which can give clear signatures about the Griffiths phase[23]. Combining this with the fact that the Griffiths phase can indeed make itself manifested in disordered dielectrics[24] makes this double perovskite an interesting candidate to carry out microscopic measurements, for example using neutrons, to understand the magnetic and dielectric properties in more detail. Impedance spectroscopy and modified-Debye model is used to analysis the dielectric response and identified a characteristic temperature that separates two regions of dielectric relaxation. This allows us to postulate a close correlation between magnetic, electronic and dielectric properties in this compound.

IV. ACKNOWLEDGEMENTS

SE wishes to acknowledge Department of Science and Technology, India for financial support. HN wishes to acknowledge Aditya Wagh for his help and support with dielectric measurements.

[1] R. I. Dass, J. Q. Yan, and J. B. Goodenough, Phy. Rev. B **68**, 064415 (2003).
[2] N. S. Rogado, J. Li, A. W. Sleight, and M. A. Subramanian, Adv. Mater. **17**, 2225 (2005).
[3] M. P. Singh, C. Grygiel, W. C. Sheets, P. Boullay, M. Hervieu, W. Prellier, B. Mercey, C. Simon, and B. Raveau, Appl. Phys. Lett. **91**, 012503 (2007).
[4] S. Kumar, G. Giovannetti, and S. van den Brink, J.and Picozzi, Phys. Rev. B **82**, 134429 (2010).
[5] S. Yáñez Vilar, E. D. Mun, V. S. Zapf, B. G. Ueland, J. S. Gardner, J. D. Thompson, J. Singleton, M. Sánchez-Andújar, J. Mira, N. Biskup, M. A. Señarís Rodríguez, and C. D. Batista, Phys. Rev. B **84**, 134427 (2011).
[6] P. Padhan, H. Z. Guo, P. LeClair, and A. Gupta, App. Phys. Lett. **92**, 022909 (2008).

[7]Y. Q. Lin, X. M. Chen, and X. Q. Liu, Solid State Commun. **149**, 784 (2009).
[8]H. S. Nair, D. Swain, N. Hariharan, S. Adiga, C. Narayana, and S. Elizabeth, J. Appl. Phys. **110**, 123919 (2011).
[9]R. Schmidt, J. Ventura, E. Langenberg, N. M. Nemes, C. Munuera, M. Varela, M. Garcia-Hernandez, C. Leon, J. Santamaria, and T. Kelvin, Phy. Rev. B **86**, 035113 (2012).
[10]A. J. Baron-Gonzalez, C. Frontera, J. L. Gracía-Muñoz, and J. Rivas-Murias, Band Blasco, J. Phys.: Condens. Matter **23**, 496003 (2011).
[11]R. Schmidt, W. Eerenstein, T. Winiecki, F. D. Morrison, and P. A. Midgley, Phys. Rev. B **75**, 245111 (2007).
[12]P. Lunkenheimer, S. Krohns, S. Riegg, S. G. Ebbinghaus, A. Reller, and A. Loidl, Eur. Phys. J. Special Topics **89**, 61 (2010).
[13]E. Barsukov and J. Macdonald, *Impedance Spectroscopy; Theory, Ecperiment and Applications* (Wiley, Hoboken, New Jersey, 2005).
[14]J. T. S. Irvine, D. C. Sinclair, and A. R. West, Adv. Mater. **2**, 132 (1990).
[15]A. K. Jonscher, *Dielectric Relaxation in Solids* (Chelsea Dielectric Press, London, 1983).
[16]C. H. Hsu and F. Mansfeld, Corrosios **57**, 747 (2011).
[17]J. T. S. Irvine and A. R. West, Solid State Ionics **40/41**, 220 (1990).
[18]R. K. Katare, L. Pandey, R. K. Dwivedi, O. Prakash, and D. Kumar, Indian Journal Engineering & Material Science **6**, 34 (1999).
[19]J. H. Lee, H. Chou, H. S. Hsu, C. P. Lin, and C. M. Fu, IEEE TRANSACTIONS ON MAGNETICS **44**, 11 (2008).
[20]K. S. Cole and R. H. Cole, J. Chem. Phys. **9**, 341 (1941).
[21]M. G. Masud, A. Ghosh, J. Sannigrahi, and B. K. Chaudhuri, J. Phys.: Condens. Matter **24**, 295902 (2012).
[22]Y. Q. Lin and X. M. Chen, J. Am. Ceram. Soc. **94**, 782 (2011).
[23]J. Deisenhofer, D. Braak, H. A. K. von Nidda, J. Hemberger, R. M. Eremina, V. A. Ivanshin, A. M. Balbashov, G. Jug, A. Loidl, T. Kimura, and Y. Tokura, Phys. Rev. Lett. **95**, 257202 (2005).
[24]V. A. Stephanovich, Eur. Phys. J. B **18**, 17 (2000).